

Spin-orbital glass transition in a model frustrated pyrochlore magnet without quenched disorder

Kota Mitsumoto,¹ Chisa Hotta,² and Hajime Yoshino^{3,1}

¹*Graduate School of Science, Osaka University, Toyonaka, Osaka 560-0043, Japan*

²*Department of Basic Science, University of Tokyo, Tokyo 153-8902, Japan*

³*Cybermedia Center, Osaka University, Toyonaka, Osaka 560-0043, Japan*

We show theoretically that spin and orbital degrees of freedom in the pyrochlore oxide $\text{Y}_2\text{Mo}_2\text{O}_7$, which is free of quenched disorder, can exhibit a simultaneous glass transition, working as dynamical randomness to each other. The interplay of spins and orbitals is mediated by the Jahn-Teller lattice distortion that selects the choice of orbitals and vary the sign of the spin exchange interactions. Our Monte Carlo simulations detect the power-law divergence of the relaxation times and the negative divergence of both the magnetic and dielectric susceptibilities, resolving the long-standing puzzle on the origin of the disorder-free spin glass.

The spin glass (SG) is one of the large family members of the low temperature thermodynamic phase of matter known as a cooperative paramagnet, including spin liquid, valence bond states, spin ice, and so on[1]. In classical antiferromagnets on triangular, kagome and pyrochlore lattices, the frustration among interactions caused by the lattice geometry precludes the possibility of all bonds to be simultaneously satisfied in energy[2], and the system comprises a macroscopically degenerate, flat energy landscape. In most cases, the subdominant effects such as quantum or thermal fluctuations and lattice distortions lift these degeneracies and drive the system to a long range order or some exotic paramagnets. When the quenched disorder is introduced, the flat energy landscape develops into an irregular structure with a huge number of quasi-degenerate minima, which is considered to be the feature of the SG as an exotic classical, cooperatively frozen paramagnet.

In contrast to the divergent behavior of the magnetic susceptibility at the conventional magnetic transition, only a cusp is observed at the SG transition, while instead the divergent *nonlinear susceptibility* is expected [3–5]. Although the SG transition is known from 1970's its origin still remains intriguing; It is observed not only in the so-called canonical SGs with strong chemical disorder [3] but also in frustrated magnets with a small amount of chemical disorder [6–8]. In theories, only the models with strong quenched disorder represented by the Edwards Anderson model [4, 5, 9–11] are known to realize the finite temperature thermodynamic SG transition. However, there is another class of pyrochlore systems *free of disorder*, exhibiting a very sharp SG transition[12–19], which is indistinguishable from the conventional one with quenched disorder.

The Letter aims to clarify the origin of the SG transition in the disorder-free pyrochlore magnets by constructing a realistic model consisting of spin and orbital degrees of freedoms. The two degrees of freedom correlate as dynamical randomness to each other and simultaneously freeze into the disordered state. So far, ideal ther-

modynamic glass transition without quenched randomness is theoretically established only in infinite dimensions within the scheme of mean-field theories for structural glasses [20–22] and spin models with large number of components [23]. Our model provides such a novel class of SG out of multi-degrees of freedom in crystalline solids that can be tested in laboratories.

The prototypical materials for our theory are the pyrochlore oxides, $\text{A}_2\text{Mo}_2\text{O}_7$ ($\text{A} = \text{Ho}, \text{Y}, \text{Dy}, \text{Tb}$), which are insulating and show a SG transition at around 20K[15, 16, 24–27]. The magnetic ions Mo^{4+} sit on the vertices of the corner shared tetrahedra (see Fig. 1(a)), and the interactions between them are antiferromagnetic, whose underlying microscopic mechanism is the superexchange mediated by the O^{2-} ions[28]. It has been established that the classical spin model with purely antiferromagnetic nearest neighbor interactions on the pyrochlore lattice remains nonmagnetic down to zero temperature because of the strong frustration effect[29, 30], not providing any hint of the SG transitions observed in experiments.

Very recently, some salient features of the local lattice distortions in $\text{Y}_2\text{Mo}_2\text{O}_7$ [31] were uncovered experimentally. The analysis based on the neutron pair-distribution function data suggests that the Mo^{4+} ions are locally displaced towards (*in*) or away from (*out*) the centers of Mo_4 tetrahedra (see Fig. 1(a)), explaining well a large variance of the Mo-Mo distances observed in the X-ray absorption study[32]. A natural mechanism of distortion is the Jahn-Teller (JT) effect that lowers the electrostatic energy of the Mo ion lifting its orbital degeneracy [33]. The displacements of the four Mo^{4+} ions on each tetrahedron possibly follow the 2-in-2-out rule, i. e. the ice-rule (see Fig. 1(a,b)), generating huge numbers of ionic configurations over the system equivalent in their JT energies. Such distortions thus do not lead to any long-range structural ordering.

It is empirically known [34] that the exchange interaction may vary significantly and even changes its sign, depending on the degree of the Mo-O-Mo angle α [28].

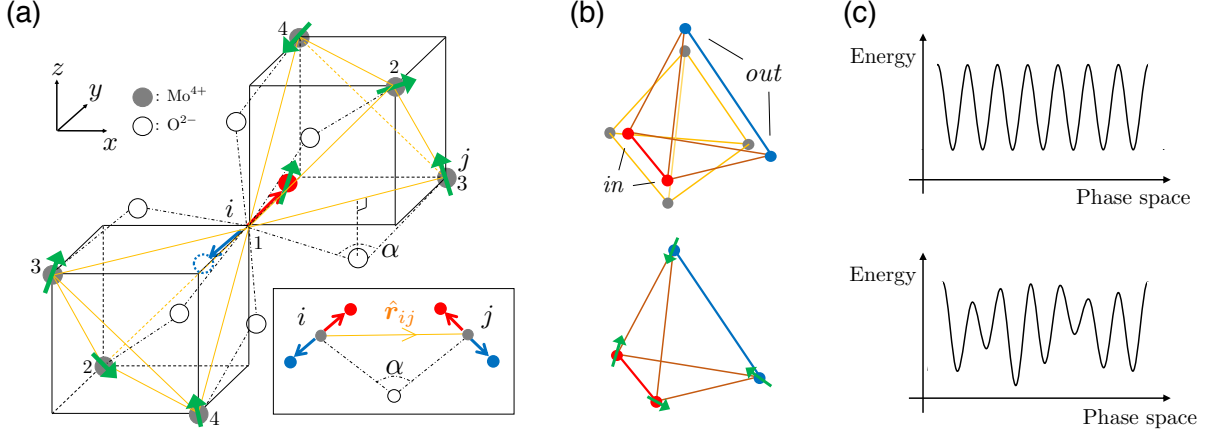


FIG. 1. (a): O²⁻ ions and magnetic Mo⁴⁺ ions around the *i* site. The numbers near the Mo⁴⁺ ions denote the sublattice to which they belong. The red and blue dashed circles represent the positions of the Jahn-Teller distorted *i* ion. We pick up the *i, j* ions and the mediated O²⁻ and draw it in the small window. α represents the angle of Mo-O-Mo and \hat{r}_{ij} represents the unit vector from the *i* site to the *j* site. (b): Ice-type displacements of the Mo₄ tetrahedron. The different color bonds represent different exchange interactions. (c): Schematic pictures of the energy landscape of ice-type displacements (Top) and modified one by the coupling between the spin and lattice distortion.

Indeed, the angle evaluated from the variance of the displacements of the Mo ions distributes in the range $\alpha = 116^\circ$ and 139° , which is large enough to change the sign of the interaction. Then, depending on the configurations of the local lattice distortion in space, the magnetic exchange interaction may acquire a random distribution with finite variances. This can be thought of as follows; If we consider the Jahn-Teller Hamiltonian including only the lattice degrees of freedom, the energy landscape should be such that all the ice-rules give the energy minima of the same height (see Fig. 1(c)) [35, 36]. In putting spins on the ice-type displaced vertices, its energy landscape is modified to an irregular one with random valley structures, since the variance of the spin interactions from ferro to antiferromagnetic ones add different energies to each ice configuration. We verify the above picture showing numerically that the spin and lattice distortions simultaneously undergo a glass transition and freeze into the aperiodic, irregular types of configuration. Since the randomly frozen lattice distortions indicate the randomly selected orbital configurations, we call it a *spin-orbital glass*.

As a natural description of the material faithful to the experimental observations, we introduce a disorder-free spin model including not only the classical Heisenberg spins \mathbf{S}_i ($i = 1, 2, 3, \dots, N$) for the magnetic moments of the Mo⁴⁺ ions but also the degree of lattice distortion of the Mo ions σ_i represented as vectors taking two discrete values, $\sigma_i = \sigma_i \hat{e}_\nu$. Here, $\sigma_i = \pm 1$ corresponds to either *in* or *out* depending on the direction of \hat{e}_ν which is the unit vector in the $[111]$, $[\bar{1}\bar{1}\bar{1}]$, $[\bar{1}11]$ and $[1\bar{1}\bar{1}]$ directions, respectively for the sublattices $\nu = 1, 2, 3, 4$ which the *i*-th spin belongs to (See Fig. 1(a)). The Hamiltonian is

given by

$$H = \sum_{\langle ij \rangle} J_{\sigma_i, \sigma_j} \mathbf{S}_i \cdot \mathbf{S}_j - \epsilon \sum_{\langle ij \rangle} \sigma_i \cdot \sigma_j \quad (\epsilon > 0) \quad (1)$$

with

$$J_{\sigma_i, \sigma_j} = J[1 + \delta(\hat{r}_{ij} \cdot \sigma_i + (-\hat{r}_{ij}) \cdot \sigma_j)] \quad (\delta > 0), \quad (2)$$

The first term in Eq. (1) represents the exchange interaction whose coupling constant J_{σ_i, σ_j} depends on the angle of Mo-O-Mo bond. We assume that the coupling constant is determined by the inner products $\hat{r}_{ij} \cdot \sigma_i$ and $\hat{r}_{ij} \cdot \sigma_j$ with the amplitude δ , where \hat{r}_{ij} is the unit vector from *i*-th site to *j*-th site. Then the coupling constant takes three kinds of value such that $J_{\sigma_i, \sigma_j} = (1 + 2\tilde{\delta})J$ (*in, in*), J (*in, out*), $(1 - 2\tilde{\delta})J$ (*out, out*), where $\tilde{\delta} = \sqrt{6}\delta/3$ (See Fig. 1(b)). The second term of Eq. (1) represents the elastic energy of the Mo⁴⁺ displacement. The elastic energy takes the minima if a Mo⁴⁺ tetrahedron satisfies the ice-rule. More precisely, the elastic energy of each bond takes $\epsilon \sigma_i \cdot \sigma_j = -\epsilon/3$ if both displacements are *out* or *in*, otherwise $+\epsilon/3$. [37] There are three parameters in this system; $\tilde{T} = k_B T/J$ is dimensionless temperature, $\tilde{\epsilon} = \epsilon/3J$ the ratio of the energy scales between the exchange interaction and the elastic energy of the displacement, and $\tilde{\delta} = \sqrt{6}\delta/3$ is the amplitude of the displacement (hereafter we call them simply as T , ϵ , δ). At $\epsilon \rightarrow \infty$, the lattice distortion becomes static. In the following analysis, we mainly focus on a representative system at $\delta = 1.5$, $\epsilon = 0.6$. We consider the periodic systems of cubic geometry with L^3 unit cells with totally $N = 16L^3$ spins, and perform 120 statistically independent runs for the system size $L = 4, 5, 6, 8$, evaluating the averages and mean-squared errors of ob-

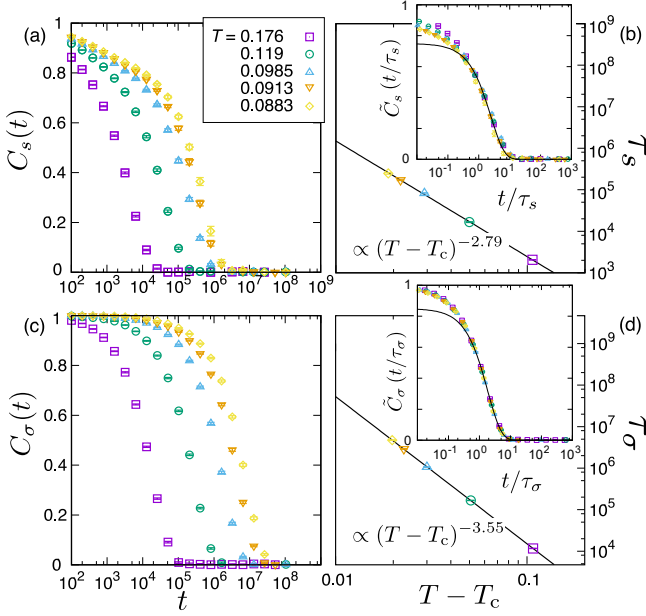


FIG. 2. Dynamical observables for $L = 6$. (a): Spin auto-correlation function. (b): Typical relaxation time of spin variables. (c): Orbital auto-correlation function. (d): Typical relaxation time of orbital variables. The black solid lines in the figure (b) and (d) denote the fits by $\tau = A(T - T_c)^{-z\nu}$ with $(A, T_c, z\nu)_s = (3.99(89), 0.0695(19), 2.79(12))$ and $(A, T_c, z\nu)_\sigma = (4.27(31), 0.0686(5), 3.55(4))$ by using the least squares method. Insets: Scaling plots of auto-correlation functions using their relaxation times. The solid lines represent the exponential fits.

servables. To equilibrate the system we made a combined use of the exchange Monte Carlo method[38, 39], conventional and loop[40] update for lattice variables, Metropolis-Reflection[41] and over-relaxation[42] update for spin variables. We took 3×10^7 Monte Carlo steps for both equilibration and for taking thermal averages $\langle \dots \rangle_{\text{eq}}$.

To explore spin and orbital freezing we examined the auto-correlation functions (ACF) for both degrees of freedom defined as $C_s(t) = N^{-1} \sum_{i=1}^N \mathbf{S}_i(t) \cdot \mathbf{S}_i(0)$ and $C_\sigma(t) = N^{-1} \sum_{i=1}^N \boldsymbol{\sigma}_i(t) \cdot \boldsymbol{\sigma}_i(0)$. The behavior of the spin and orbital ACFs are shown in Figs. 2(a) and 2(c). Both ACFs indicates the slowing down of the dynamics. As a quantitative measure of dynamics, we define the relaxation times $\tau_s(T)$ and $\tau_\sigma(T)$ for each degree of freedom as the timescale such that the ACFs decrease down to 0.5, which are evaluated as shown in Figs. 2(c) and 2(d). Both relaxation times diverge at the same temperature $T_c \approx 0.07$ with power laws although their exponents differ. This suggests that spin and orbital are frozen simultaneously. We checked that there is no finite size effect within the time scale which we analyzed. In the insets of Figs. 2(c) and 2(d) we show the scaling plots of ACFs assuming a scaling form, $C(t, T) = \tilde{C}(t/\tau(T))$, which is clearly satisfied. The scaling functions turns out to be well fitted by simple exponentials. We note that

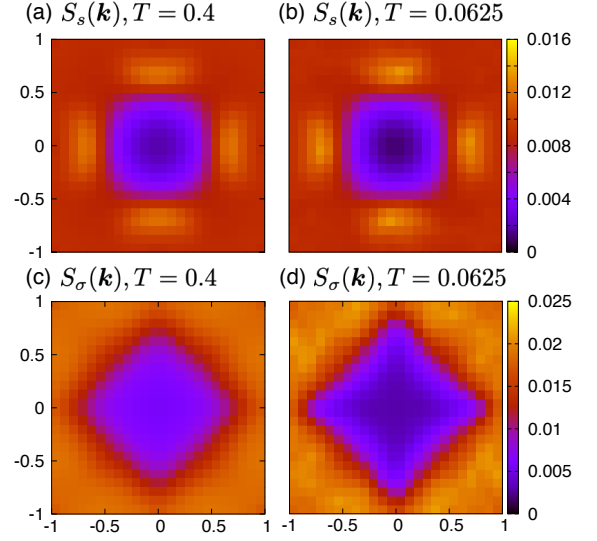


FIG. 3. Structure factors for $L = 6$ on the $(k_y/\pi)-(k_z/\pi)$ plane. (a) and (b) show the spin and orbital(lattice distortion) structure factors at $T = 0.4$, respectively. (c) and (d) show the structure factors at $T = 0.0625$, respectively.

the relaxation function in the Edwards-Anderson models in the paramagnetic phase is more complicated [43, 44] presumably due to Griffith singularity [45].

Next, we analyze the static-structure factors of spins and lattice distortions defined respectively as $S_s(\mathbf{k}) = N^{-1} |\sum_{i=1}^N e^{-i\mathbf{k} \cdot \mathbf{r}_i} \mathbf{S}_i \cdot \mathbf{S}_i|$ and $S_\sigma(\mathbf{k}) = N^{-1} |\sum_{i=1}^N e^{-i\mathbf{k} \cdot \mathbf{r}_i} \boldsymbol{\sigma}_i \cdot \boldsymbol{\sigma}_i|$, where \mathbf{k} is a wave vector. In figures 3(a) and 3(b) we show $S_s(0, k_y, k_z)$ above and below T_c . There is no notable difference between the two. The Bragg peak is not observed below T_c , indicating that there is no magnetic long range order. In Figs. 3(c) and 3(d), we also find no sign of long range order in the lattice distortions, although the short range order seems to develop at a lower temperature. We also note that the fraction of tetrahedra that satisfy the ice-rule increases smoothly with decreasing temperature without any anomaly at the transition temperature T_c . (see SI).

The present SG transition can be detected by the two thermodynamic quantities. One is the nonlinear magnetic susceptibility,

$$\chi_3 = \frac{1}{3} \sum_{\mu} \frac{\partial^3 \langle m_{\mu} \rangle_{\text{eq}}}{\partial h_{\mu}^3} \bigg|_{h_{\mu} \rightarrow 0}, \quad (3)$$

where $m_{\mu} = N^{-1} \sum_{i=1}^N S_{i\mu}$ and h_{μ} are the magnetization and the magnetic field, respectively, in the μ -direction ($\mu = x, y, z$). The other is the nonlinear dielectric susceptibility,

$$\chi_3^{\sigma} = \frac{1}{4} \sum_{\nu} \frac{\partial^3 \langle p_{\nu} \rangle_{\text{eq}}}{\partial E_{\nu}^3} \bigg|_{E_{\nu} \rightarrow 0}, \quad (4)$$

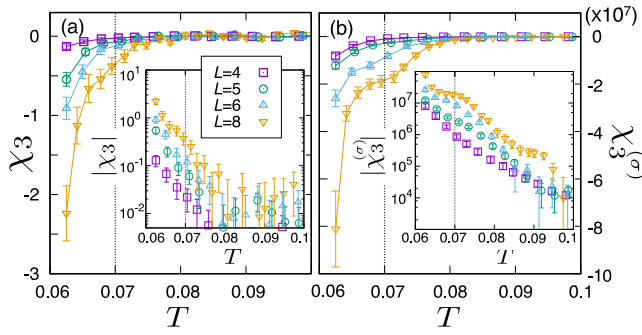


FIG. 4. (a), (b): Size dependence of nonlinear magnetic and dielectric susceptibilities (Insets: logarithmic scale of absolute values). The dashed line represents the freezing temperature $T_c \approx 0.07$ determined by the auto-correlation function.

where $p_\nu = N^{-1} \sum_{i=1}^N \sigma_i \cdot \hat{e}_\nu$ is the dielectric polarization in the \hat{e}_ν -direction and E_ν is the electric field. Fortunately, since Mo^{4+} ion has an electric charge, the fluctuation of the orbital glass ordering can be detected electrically. Thus, the two quantities are measurable in laboratories and allow a direct comparison between theories and experiments. In conventional theories [10, 11], one often analyzes the SG susceptibility, χ_{SG} , which is proportional to χ_3 . Although χ_{SG} is much easier to calculate with better accuracy in the presence of quenched disorder by using the overlap between two independent replicas, it is not convenient for our model, since the Hamiltonian is translationally invariant so that the replicas usually do not overlap.

Figure 4(a) shows χ_3 as a function of temperature for several system size L . In overall, it takes the negative value, and from slightly above T_c , its amplitude starts to grow rapidly in lowering the temperature. This growth is enhanced for larger L , strongly suggesting that the divergence of χ_3 remains in the thermodynamic limit, which is consistent with the experimental observation in $\text{Y}_2\text{Mo}_2\text{O}_7$. Similar behavior is observed for $\chi_3^{(\sigma)}$, indicating the freezing of the orbital degrees of freedom into a disordered state.

Let us discuss the relevance of our results with experiments. The existence of the SG transition itself is already established in $\text{Y}_2\text{Mo}_2\text{O}_7$ and its families, and although its origin has not been understood, a recent analysis showed that the lattice distortions possibly plays a certain role in the glass transition. Our model is constructed based on this finding by including the direct coupling between the lattice distortion and the spin. The two degrees of freedom simultaneously undergo a glass transition, indicating that they generate an effect of dynamical randomness to each other. Experiments can test our scenario by examining whether the nonlinear dielectric susceptibility diverges in the vicinity of T_c , where already the nonlinear magnetic susceptibility shows the divergence. Previously, the orbital-glass transition was observed in the

FeCr_2S_4 , where the dielectric spectroscopy measurement played a major role, detecting the slowing down of orbital dynamics [46]. Similar techniques shall be applied to the pyrochlore materials.

Let us finally comment on the scenario often posed experimentally, which expects the freezing of the orbital degrees of freedom at a higher temperature than the SG transition [31, 32]. Once the orbital configuration is frozen, our model is reduced to the standard EA model of Heisenberg spins with quenched randomness on a pyrochlore lattice, which is known to exhibit a SG transition. [47, 48] Actually, if we increase ϵ in Eq.(1), the ice-rule configuration of orbitals is selected at the higher temperature, which is detected by the broad peak in the heat capacity (see SI). However, this peak does not mean the transition but a crossover; Below that temperature, the orbitals are still dynamically fluctuating among huge numbers of quasi-degenerate ice-rule configurations. In lowering the temperature, the orbital dynamics naturally slows down but without any thermodynamic anomaly much as usual spin ices [49]. Interestingly, at a lower temperature the heat capacity shows a second peak (see SI) which should be attributed to coupling between the spin and lattice distortions. In our scenario, we anticipate the thermodynamic spin-orbital glass transition at around that temperature.

Some other effect such as the spin-orbit interaction, the spin-phonon coupling and longer range interactions, which are not included in our model, may play a secondary role to reproduce more precisely the experimental measurements, whereas our findings proved that the interplay of nearest-neighbor interactions and the dynamical JT distortions can solely drive the system to the glass transition. The present model can be further applied to other SG frustrated magnets such as $\text{Tb}_2\text{Mo}_2\text{O}_7$ whose magnetic ion is JT active.

To summarize, we introduced the realistic model without quenched randomness consisting of spin and orbital degrees of freedom, that shows the thermodynamic glass transition for the first time in the finite dimensional periodic lattice. We performed the dynamical simulations in the equilibrium and found that the relaxation times of both spins and orbitals show a power-law divergence at the same temperature, T_c . The nonlinear magnetic susceptibility and the nonlinear dielectric susceptibility together show negative divergence at around T_c , signaling the simultaneous glass transition of these two degrees of freedom. The former is consistent with the experiments already performed in the pyrochlore oxide, $\text{Y}_2\text{Mo}_2\text{O}_7$, whereas the latter can be tested in the near future to fix the long standing problem on the origin of the SG transition in this disorder free crystalline solid.

This work was supported by KAKENHI (No. 19H01812, 17K05533, 17K05497, 18H01173, 17H02916) from MEXT, Japan. The computation in this work has been done using the facilities of the Supercomputer Cen-

ter, the Institute for Solid State Physics, the University of Tokyo, OCTOPUS and supercomputer system SX-ACE at the Cybermedia Center, Osaka University.

-
- [1] J. Gardner, M. Gingras, and J. Greedan, *Reviews of Modern Physics* **82**, 53 (2010).
 - [2] H. Diep *et al.*, (World Scientific, 2013).
 - [3] J. Mydosh, (CRC Press, 2014).
 - [4] K. Binder and A. Young, *Reviews of Modern physics* **58**, 801 (1986).
 - [5] H. Kawamura and T. Taniguchi, *Handbook of Magnetic Materials*, Vol. 24 (Elsevier, 2015) pp. 1–137.
 - [6] A. Ramirez, G. Espinosa, and A. Cooper, *Physical review letters* **64**, 2070 (1990).
 - [7] H. Martinho and et al., *Physical review B* **64**, 024408 (2001).
 - [8] N. Tristan and et al., *Physical Review B* **72**, 174404 (2005).
 - [9] S. Edwards and P. Anderson, *Journal of Physics F: Metal Physics* **5**, 965 (1975).
 - [10] M. Mézard, G. Parisi, and M. Virasoro, Vol. 9 (World Scientific Publishing Company, 1987).
 - [11] D. Fisher and D. Huse, *Physical Review B* **38**, 386 (1988).
 - [12] M. Alba, J. Hammann, C. Jacoboni, and C. Pappa, *Physics Letters A* **89**, 423 (1982).
 - [13] J. Greedan, M. Sato, X. Yan, and F. Razavi, *Solid state communications* **59**, 895 (1986).
 - [14] J. Reimers, J. Greedan, R. Kremer, E. Gmelin, and M. Subramanian, *Physical Review B* **43**, 3387 (1991).
 - [15] M. Gingras, C. Stager, N. Raju, B. Gaulin, and J. Greedan, *Physical review letters* **78**, 947 (1997).
 - [16] J. Gardner and et al., *Physical review letters* **83**, 211 (1999).
 - [17] H. Zhou, C. Wiebe, A. Harter, N. Dalal, and J. Gardner, *Journal of Physics: Condensed Matter* **20**, 325201 (2008).
 - [18] T. Taniguchi, T. Munenaka, and H. Sato, in *Journal of Physics: Conference Series*, Vol. 145 (IOP Publishing, 2009) p. 012017.
 - [19] F. Ladieu, F. Bert, V. Dupuis, E. Vincent, and J. Hammann, *Journal of Physics: Condensed Matter* **16**, S735 (2004).
 - [20] G. Parisi and F. Zamponi, *Reviews of Modern Physics* **82**, 789 (2010).
 - [21] J. Kurchan, G. Parisi, and F. Zamponi, *Journal of Statistical Mechanics: Theory and Experiment* **2012**, P10012 (2012).
 - [22] P. Charbonneau, J. Kurchan, G. Parisi, P. Urbani, and F. Zamponi, *Nature communications* **5** (2014).
 - [23] H. Yoshino, *SciPost Physics* **4**, 040 (2018).
 - [24] B. Gaulin, J. Reimers, T. Mason, J. Greedan, and Z. Tun, *Physical review letters* **69**, 3244 (1992).
 - [25] S. Dunsiger and et al., *Physical Review B* **54**, 9019 (1996).
 - [26] I. Kézsmárki and et al., *Physical review letters* **93**, 266401 (2004).
 - [27] N. Hanasaki and et al., *Physical review letters* **99**, 086401 (2007).
 - [28] I. Solovyev, *Physical Review B* **67**, 174406 (2003).
 - [29] J. Reimers, A. Berlinsky, and A. Shi, *Physical Review B* **43**, 865 (1991).
 - [30] R. Moessner and J. Chalker, *Physical review letters* **80**, 2929 (1998).
 - [31] P. Thygesen and et al., *Physical review letters* **118**, 067201 (2017).
 - [32] C. Booth and et al., *Physical Review B* **62**, R755 (2000).
 - [33] A magnetic Mo^{4+} ($4d^2$, spin $S = 1$) ion is affected by the trigonal crystal field of MoO_6 and then its three t_{2g} orbitals are split to a_{1g} orbital and doubly degenerated e'_g orbitals. An electron is in lower a_{1g} and the other is in e'_g with same directions (Hund's rule). Hence the e'_g -doublet becomes JT active.
 - [34] The evaluation of the direct exchange interactions between Mo spins can be done based on the Hartree-Fock approach by assuming the orbital ordering, which gives a rough estimate of the sign of the interactions. We give a more detailed analysis by considering the dominant superexchange interactions for the insulating $\text{Y}_2\text{Mo}_2\text{O}_7$.
 - [35] L. Pauling, Vol. 260 (Cornell university press Ithaca, NY, 1960).
 - [36] S. Bramwell and M. Gingras, *Science* **294**, 1495 (2001).
 - [37] This term is the simplified description of the energies of the classical elastic model whose lattice sites are connected by springs, for which one can easily find that the two-in two-out configurations give the lowest energy, consistent with the experimental findings.
 - [38] K. Hukushima and K. Nemoto, *Journal of the Physical Society of Japan* **65**, 1604 (1996).
 - [39] K. Hukushima, *Physical Review E* **60**, 3606 (1999).
 - [40] R. Melko, B. den Hertog, and M. Gingras, *Physical review letters* **87**, 067203 (2001).
 - [41] S. Pawig and K. Pinn, *International Journal of Modern Physics C* **9**, 727 (1998).
 - [42] J. Alonso and et al., *Physical Review B* **53**, 2537 (1996).
 - [43] A. Ogielski, *Physical Review B* **32**, 7384 (1985).
 - [44] H. Yoshino and H. Takayama, *EPL (Europhysics Letters)* **22**, 631 (1993).
 - [45] A. Bray, *Physical review letters* **60**, 720 (1988).
 - [46] R. Fichtl and et al., *Physical review letters* **94**, 027601 (2005).
 - [47] T. Saunders and J. Chalker, *Physical review letters* **98**, 157201 (2007).
 - [48] H. Shinaoka, Y. Tomita, and Y. Motome, *Physical review letters* **107**, 047204 (2011).
 - [49] L. Jaubert and P. Holdsworth, *Nature Physics* **5**, 258 (2009).

Details of Monte Carlo simulation

Equilibration and measurements of static quantities

For updating the lattice distortions σ_i ($i = 1, 2, 3, \dots, N$) we used the conventional single-spin-flip Metropolis method. However, it is hard to equilibrate the ice-like system at low temperatures due to multiple energy minima with high energy barriers. Therefore, we also adopted the standard nonlocal update method called as the loop algorithm. [40] The nonlocal updates consisted of two steps: (1) We look for a loop composed of only *in-out* bonds. (2) We flip all the lattice distortions along the selected loop simultaneously with the acceptance rate determined by the Metropolis rule. Note that the energy contributed by the second term of the Hamiltonian is unchanged in this update.

For updating the Heisenberg spins we used the Metropolis Reflection method [41] and the over-relaxation method. [42] In the Metropolis Reflection method, we choose a plane which divides the spin space into two halves, randomly. To update a spin \mathbf{S}_i , a new candidate spin configuration \mathbf{S}'_i is created by reflecting \mathbf{S}_i by the plane. More precisely the sign of the spin component perpendicular to plane is changed. The reflection is performed with probability determined by Metropolis rule. In a unit Monte Carlo step (MCS), we try the updates for all spins \mathbf{S}_i ($i = 1, 2, 3, \dots, N$) using the same reflection plane. The reflection plane itself is updated once in 1 MCS. In the over-relaxation method, we first compute the effective magnetic field \mathbf{h}_{eff} around a spin \mathbf{S}_i , and then rotate the spin around \mathbf{h}_{eff} by an angle of π .

To summarize, a unit Monte Carlo step consists of the following steps.

1. Sequential single-spin flips for all lattice distortions with the conventional Metropolis method
2. L times loop updates for lattice distortions
3. Compute all the coupling constants J_{σ_i, σ_j}
4. Sequential single-spin flips for all Heisenberg spins with the Metropolis Reflection method
5. L times sequential single-spin flips for all Heisenberg spins with the over-relaxation method

Here L is the system size defined in the main text.

On top of the steps 1-5, we add the replica exchange method. [38, 39] We used 48 replicas for $L = 4, 5, 6$ and 72 replicas for $L = 8$. We chose the maximum temperature and the minimum temperature as $T_{\text{max}} = 0.400$ and $T_{\text{min}} = 0.0625$ respectively. We optimized the set of temperatures between T_{max} and T_{min} such that the exchange rate becomes the same for all temperatures. [39]

We performed one trial to exchange the replicas once in each interval of 15 (MCS).

Initial spin and lattice configuration for each replica were prepared as fully random configurations. MCSs for thermalization was chosen as 3.0×10^7 (MCS) for all system sizes. Observations of physical quantities are made during additional 3.0×10^7 (MCS) to evaluate their thermal averages $\langle \dots \rangle_{\text{eq}}$ by the Monte Carlo simulation.

Measurements of dynamic quantities

To measure dynamical quantities in equilibrium, the initial configurations ($t = 0$ (MCS)) are created by the method explained above. In order to observe the natural time evolution we apply *only* the sequential single-spin flip for both degrees of freedom switching off other methods. A unit Monte Carlo step then consists of the following steps.

1. Sequential single-spin flip for all lattice distortions with the conventional Metropolis method
2. Compute all the coupling constants J_{σ_i, σ_j}
3. Sequential single-spin flip for all Heisenberg spins with the Metropolis Reflection method

Nonlinear susceptibility

The fluctuation formulae for the nonlinear magnetic susceptibility is obtained as,

$$\begin{aligned} \chi_3 &= \frac{1}{3} \sum_{\mu} \frac{\partial^3 \langle m_{\mu} \rangle_{\text{eq}}}{\partial h_{\mu}^3} \\ &= \frac{\beta^3 N^3}{3} \sum_{\mu} \left(\langle m_{\mu}^4 \rangle_{\text{eq}} - 4 \langle m_{\mu} \rangle_{\text{eq}} \langle m_{\mu}^3 \rangle_{\text{eq}} \right. \\ &\quad \left. - 3 \langle m_{\mu}^2 \rangle_{\text{eq}}^2 + 12 \langle m_{\mu}^2 \rangle_{\text{eq}} \langle m_{\mu} \rangle_{\text{eq}}^2 - 6 \langle m_{\mu} \rangle_{\text{eq}}^4 \right). \end{aligned} \quad (5)$$

In this study, the odd order moments of the magnetization become 0 from its rotational symmetry, e.g. $\langle m_{\mu} \rangle_{\text{eq}} = \langle m_{\mu}^3 \rangle_{\text{eq}} = 0$. Hence we calculate them for simply as

$$\chi_3 = \frac{\beta^3 N^3}{3} \sum_{\mu} \left(\langle m_{\mu}^4 \rangle_{\text{eq}} - 3 \langle m_{\mu}^2 \rangle_{\text{eq}}^2 \right). \quad (6)$$

We also analyzed the nonlinear dielectric susceptibility in the same manner as,

$$\chi_3^{(\sigma)} = \frac{\beta^3 N^3}{4} \sum_{\nu} \left(\langle p_{\nu}^4 \rangle_{\text{eq}} - 3 \langle p_{\nu}^2 \rangle_{\text{eq}}^2 \right). \quad (7)$$

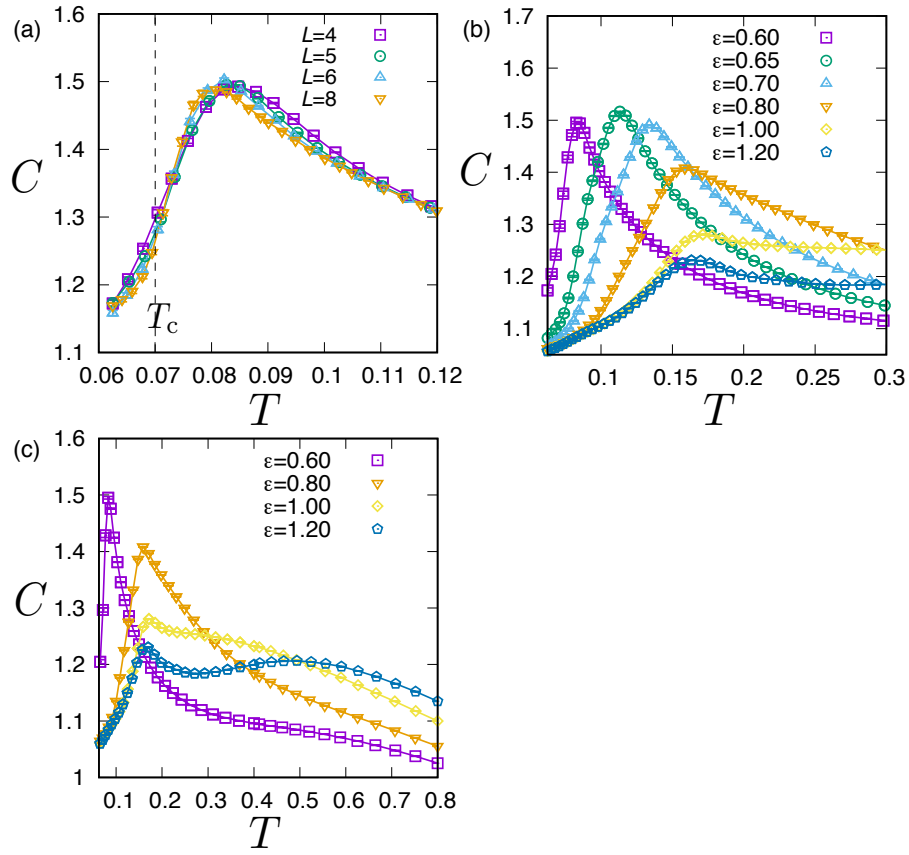


FIG. 5. Heat capacity computed as $C = N^{-1}\beta^2(\langle E^2 \rangle_{\text{eq}} - \langle E \rangle_{\text{eq}}^2)$. (a): Size dependence at $\epsilon = 0.6$. (b): ϵ dependence for $L = 5$ in the narrow temperature range of $T = 0.0625$ to $T = 0.3$. (c): ϵ dependence for $L = 5$ in the wider temperature range of $T = 0.0625$ to $T = 0.8$.

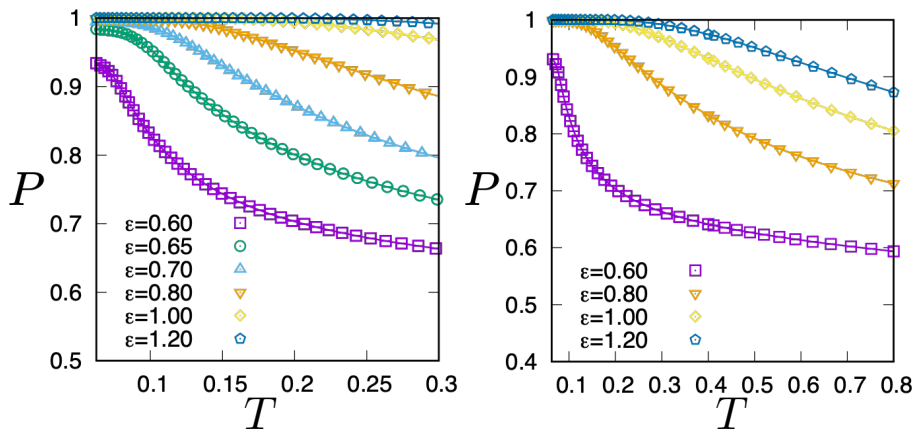


FIG. 6. Fraction of the ice structures given by $N_{2\text{-in-2-out}}/N_{\Delta}$. Here $N_{\Delta} = N_{\text{spin}}/2$ represents the number of all tetrahedra and $N_{2\text{-in-2-out}}$ represent the number of tetrahedra which are distorted into a 2-in-2-out structure. (a): ϵ dependence for $L = 5$ in the narrow temperature range of $T = 0.0625$ to $T = 0.3$. (b): ϵ dependence for $L = 5$ in the wider temperature range of $T = 0.0625$ to $T = 0.8$.

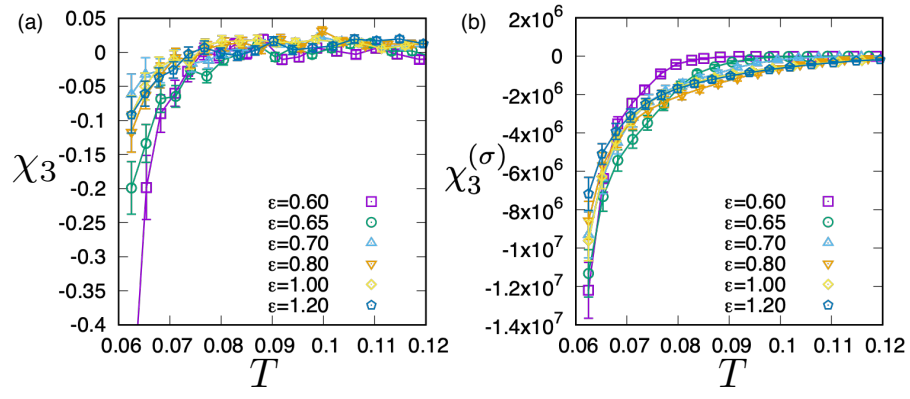


FIG. 7. (a): ϵ dependence of the nonlinear magnetic susceptibility for $L = 5$. (b): ϵ dependence of the nonlinear dielectric susceptibility for $L = 5$.